Research Square

Preprints are preliminary reports that have not undergone peer review.
They should not be considered conclusive, used to inform clinical practice,
or referenced by the media as validated information.

Simulation experimental study on fracture movement and stress evolution of overlying strata under thick hard roof

Chun Zhao
Bo Li
Yongjiang Wa
Zhenqian Ma
zqma@gzu.edu.cn

Guizhou University

Article

Keywords: thick hard roof, similar material simulation test, overlying strata fracture and movement, borehole pre-splitting weakening, stress evolution characteristics

Posted Date: November 12th, 2026

DOI: https://doi.org/10.21203/rs.3.rs-11456563/v1

License: This work is licensed under a Creative Commons Attribution 4.0 International License.
Read Full License

Additional Declarations: No competing interests reported.

Simulation experimental study on fracture movement and stress evolution of overlying strata under thick hard roof

Chun Zhao[a], Bo Li[a], Yongjiang Wan[a], Zhenqian Ma[b,*]

[a] Guizhou Bide Coal Industry Co., Ltd, Bijie City, Guizhou 553303, China;

[b] School of Mining, Guizhou University, Guiyang, Guizhou 550025, China;

* Corresponding author. E-mail address: zqma@gzu.edu.cn (Z. Ma).

Abstract: Thick and hard roofs with high strength and intact rock mass are widely distributed in the mining areas of southwestern China. Under mining disturbance, large-area suspended roofs easily form, inducing dynamic disasters such as gas over-limit, large-scale roof weighting, and roof water inrush. Taking the 40-m-thick basalt key stratum of Working Face 113203 of Songhe Coal Mine in Guizhou Province as the engineering prototype, two similar material simulation test models were constructed with two comparative working conditions: an unweakened roof and a roof weakened by borehole pre-splitting. The fracture characteristics, crack evolution patterns, and stress distribution differences of the overlying strata during working face advance were compared and analyzed. The results show that for the unweakened roof, the initial caving interval of the immediate roof is 33 m and that of the main roof is 55 m, and the periodic caving intervals of the immediate roof and the main roof are 17 m and 30 m, respectively, resulting in a large suspended roof area. After roof weakening, the initial caving interval is greatly shortened, and the roof undergoes periodic fracture along the pre-split paths for every 10 m of working face advance, effectively eliminating the hazard of large-area roof suspension. In terms of stress evolution, without pre-splitting weakening, the peak vertical stress in the coal seam reaches 0.78 MPa, with stress concentration occurring 30 m ahead of the working face. After pre-splitting weakening, the caved gangue fills the goaf in a timely manner and improves the load transfer mode of the overlying key strata; the peak vertical stress in the coal seam decreases to 0.72 MPa, and the advance influence range extends to 35 m. The research results provide experimental evidence and theoretical support for roof control and the parameter design of hydraulic fracturing pre-splitting weakening technology for working faces with basalt-type thick hard roofs in southwestern China.

Keywords: thick hard roof; similar material simulation test; overlying strata fracture and movement; borehole pre-splitting weakening; stress evolution characteristics

1. Introduction

Coal accounts for more than 50% of China's primary energy consumption, and its strategic pillar role in the national economy is irreplaceable in the short term [1-2]. Fully mechanized working faces in the mining areas of southwestern China are generally overlain by thick and hard roof strata with high integrity. These strata have high strength and strong integrity, so the roof can hardly cave immediately as mining advances and tends to form a large-scale suspended structure. When the span of the suspended roof reaches its limit value, instantaneous overall fracture occurs, and the resulting strong ground pressure disturbance can easily induce compound disasters such as rock bursts, roof water inrush, gas explosions, and coal and gas outbursts, severely constraining safe and efficient mine production [3-5]. Therefore, how to control the caving behavior of the thick hard roof and to weaken mining-induced stress concentration is a key strata control problem that urgently needs to be solved in the mining areas of southwestern China. A basalt key stratum, 40 m thick, overlies the No.32 coal seam at the 113203 working face of Guizhou Songhe Coal Industry. With a Protodyakonov firmness coefficient of, the stratum is highly integrated and hard to cave. The complex fracture and stress evolution of the mining-affected overburden poses great difficulty for in-situ roof control. Similar material simulation testing is an intuitive and effective method for studying mining-induced overlying strata movement, fracture development, and ground pressure evolution; it can fully reproduce the deformation and failure characteristics of rock strata during the entire extraction process of the working face, providing theoretical support for the development of roof control technologies [6-10].

Scholars at home and abroad have carried out extensive similar material simulation studies on thick hard roofs, mainly focusing on the fracture morphology of the overlying strata, caving intervals, and stress evolution characteristics [11-13]. Among them, Zhai Xinxian et al. [14] investigated a working face with an extra-thick conglomerate roof and revealed the caving and seismic response patterns of the overlying strata through similar simulation. Chai Jing et al. [15] integrated fiber-optic sensing and digital image correlation (DIC) optical measurement techniques to establish an integrated monitoring system for overlying strata deformation. In terms of roof cutting and pressure relief, Zhang Hanrui et al. [16] established the roof-cutting short-arm beam theory and developed key technologies of directional pre-splitting seam cutting and high-prestress support; Shi Zhihan et al. [17] verified by numerical simulation that roof cutting can significantly reduce the peak abutment stress on narrow coal pillars. Related studies show that roof cutting and pressure relief can effectively reduce roof subsidence and support intensity and improve the stability of the surrounding rock of gob-side entries [18-21]. However, existing studies mostly focus on conglomerate and sandstone hard roofs in northern mining areas, and comparative

experimental studies on basalt-type ultra-thick hard roofs in southwestern China are still scarce. Most tests only analyzed a single working condition, lacking a quantitative comparison between the two conditions of an unweakened roof and a pre-split weakened roof, and the intrinsic mechanism by which pre-splitting regulates ground pressure has not been adequately explained. Therefore, taking the engineering geological conditions of Working Face 113203 of Songhe Coal Mine as the prototype, this study constructed physical simulation models based on similarity theory, set up two comparative tests with an unweakened roof and a borehole pre-split weakened roof, quantitatively analyzed the caving intervals of the overlying strata, the fracture development morphology, and the vertical stress evolution characteristics under the two conditions, and clarified the mechanism by which borehole pre-splitting weakening regulates the ground pressure of the thick hard roof, so as to provide a scientific basis for the field application of hydraulic fracturing pre-splitting technology.

2. Engineering overview

The No. 32 coal seam of Songhe Coal Mine in Guizhou Province occurs in the Emeishan Basalt Formation, with an average dip angle of 28° and a thickness of 2.5 m. A 40-m-thick massive basalt stratum lies 17 m above the coal seam. This stratum is dense and hard with good integrity and a Protodyakonov coefficient of $f \approx 14$, and it acts as the main controlling key stratum of the working face. The in-situ stress field of the mining area is dominated by horizontal tectonic stress. The measured three-dimensional principal stresses are as follows: the maximum horizontal principal stress is 13.7–17.6 MPa with an average of 15 MPa, the minimum horizontal principal stress is 9.2–11.2 MPa with an average of 9.9 MPa, and the vertical principal stress is 10.5–13.0 MPa with an average of 11.3 MPa. The stress magnitudes satisfy $\sigma H > \sigma v > \sigma h$, indicating a typical strike-slip stress regime, and the orientation of the maximum horizontal principal stress ranges from N76.6°E to N84.5°E.

Working Face 113203, the prototype of the test, is currently under extraction, with a recoverable strike length of 790 m and an inclined length of the open-off cut of 175 m. The layout of the working face and the comprehensive stratigraphic column of its roof and floor strata are shown in Figs. 1 and 2.

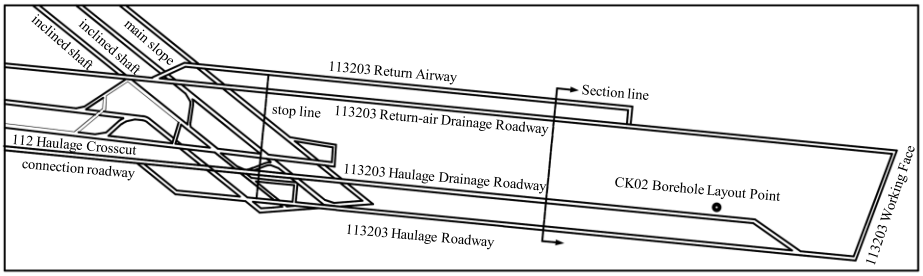


Fig. 1 Plan view of Working Face 113203

Lithologic column 1 : 200	Coal seam No.	Thickness (m) Average Min.–Max.	Lithological description
		6.11 1.79–10.45	Topsoil: yellow-green siltstone fragments.
		40.52 37.2–44.2	Basalt: green, massive; amygdaloidal in the upper part.
		3.05 2.89–3.21	Fine sandstone: gray, thick-bedded, calcareous cementation.
		0.65 0.61–0.69	Carbonaceous mudstone: black, carbonaceous.
		11.64 6.97–16.2	Siltstone: dark gray, thin-bedded, well-developed bedding.
		0.47 0.41–0.63	Sandy mudstone: dark gray.
		0.50 0.30–0.70	Carbonaceous mudstone: dark gray, massive, few plant fossils.
		0.73 0.50–0.96	Siltstone: locally wavy bedding, calcareous concretions.
	32	**2.50** 1.61–2.79	No. 32: gray-black, brown streak, semi-dull type.
		0.68 0.42–0.95	Mudstone: dark gray, massive, bauxitic spots.
		6.96 3.13–8.79	Bauxite: light gray, massive, porphyritic; pyrite.
		11.10 6.6–13.6	Tuff: purple in the upper part, amygdaloidal texture.

Fig. 2 Stratigraphic column of the roof and floor strata of the coal seam

3. physical model test method and construction procedure

3.1. Determination of similarity parameters

Based on similarity theory and the engineering geological and mechanical properties of the coal-rock mass, the geometric similarity ratio of this physical similar simulation test was set to 50 and the bulk density similarity ratio to 1.4, from which the stress similarity ratio was derived as 70. The similarity ratios of dimensionless physical quantities such as strain, Poisson's ratio, and internal friction angle were all 1.

3.2. Test materials and mix proportions

River sand was used as the skeleton material, lime and gypsum as cementing materials, and mica powder as the layer-separation material. The mix proportion of each stratum was matched to its mechanical parameters; the layer density, model thickness, and material consumption are listed in Table 1, and the raw materials are shown in Fig. 3.



(a) (b) (c) (d)

Fig. 3 Raw materials for preparing the similar material model. (a) gypsum, (b) lime,(c) river sand; (d) mica powder

Table 1 Material mix proportions for the similar material simulation test

No.	Rock stratum	Mix proportion No.	Model density/(g·cm⁻³)	Model thickness/cm	River sand/kg	Lime/kg	Gypsum/kg
1	Sandstone	429	2.77	9.0	38.39	4.32	7.46
2	Mudstone	725	2.55	3.5	13.56	2.45	2.57
3	Basalt	335	2.90	40.0	102.97	15.61	24.31
4	Siltstone	671	2.59	7.0	35.41	4.23	1.77
5	Sandy mudstone	642	2.55	2.0	11.25	2.36	2.06
6	Siltstone	671	2.59	1.0	6.14	1.29	1.80
7	Coal	753	1.40	2.5	12.31	2.01	2.86
8	Bauxite	454	3.40	5.0	31.41	8.34	4.64

3.3. Model design and loading

The model frame was designed with dimensions of 1500 mm (length) × 40 mm (width) × 1200 mm (height), rigidly constrained by a steel frame. The thickness of the strata above the top of the model exceeded the simulation range by 320 m, so a uniformly distributed hydraulic load was applied to the top of the model to equivalently simulate the self-weight stress of the overlying strata. As for the boundaries, a 15-cm-wide coal pillar (15 m in the prototype) for entry protection was reserved on each side of the model, and the open-off cut was arranged on the right side of the left coal pillar. The excavation was carried out segment by segment in a stepped manner with a single excavation length of 10 cm (10 m in the prototype) to simulate the continuous advance of the working face. The overall layout of the model is shown in Fig. 4.

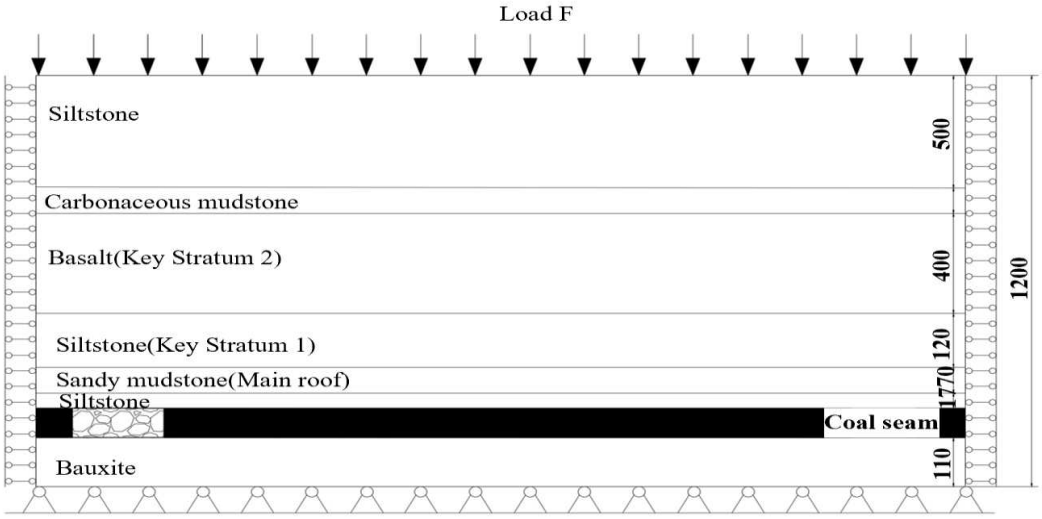


Fig. 4 Design of the similar simulation test

3.4. Layout of the data monitoring system

As shown in Fig. 5, BW-3 foil-type miniature pressure cells combined with a YJD-27 static strain indicator were used to collect vertical stress data. A total of 10 monitoring points were arranged in the coal seam, the immediate roof, the main roof, the siltstone, and the basalt key stratum, with a spacing of 25 cm along the strike direction; the points were numbered #1 – #10. In addition, the fracture morphology of the overlying strata and the crack evolution process were recorded by a high-definition camera, and the displacement field of the strata was analyzed by the speckle method.

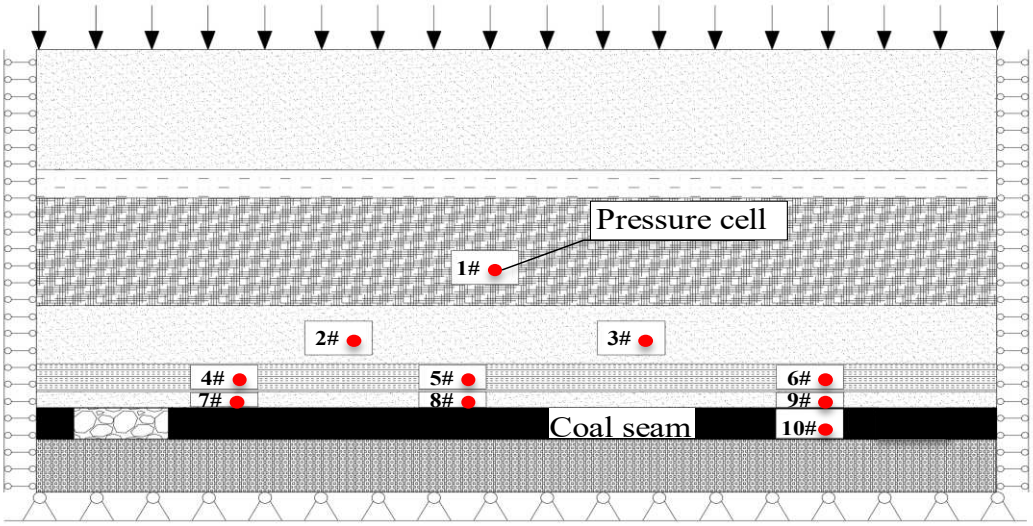


Fig. 5 Layout positions and numbering of the pressure cells

3.5. physical model construction procedure

(1) Material weighing and mixing: River sand, lime, and gypsum were weighed precisely according to the mix proportions in Table 1, dry-mixed uniformly, and then mixed with water added in stages, with the moisture content of the mixture controlled to ensure compaction and shaping.

(2) Layered placement and compaction: The mixture was placed layer by layer from bottom to top; after each layer was compacted, mica powder was spread uniformly to simulate the bedding interfaces between strata. When filling the basalt key stratum, a shaped mold was used for compaction to match the mechanical properties of the hard rock stratum.

(3) Sensor embedding: When the layered placement reached the monitoring horizons, pressure cells were embedded. Before embedding, the sensor resistance was checked to avoid poor contact and displacement under compression.

(4) Air-drying and pretreatment: After the entire model was completed, it was air-dried naturally for 23 days; latex paint was applied to the observation surface and artificial speckles were drawn, completing the pretreatment before the test.

4. Test results and analysis

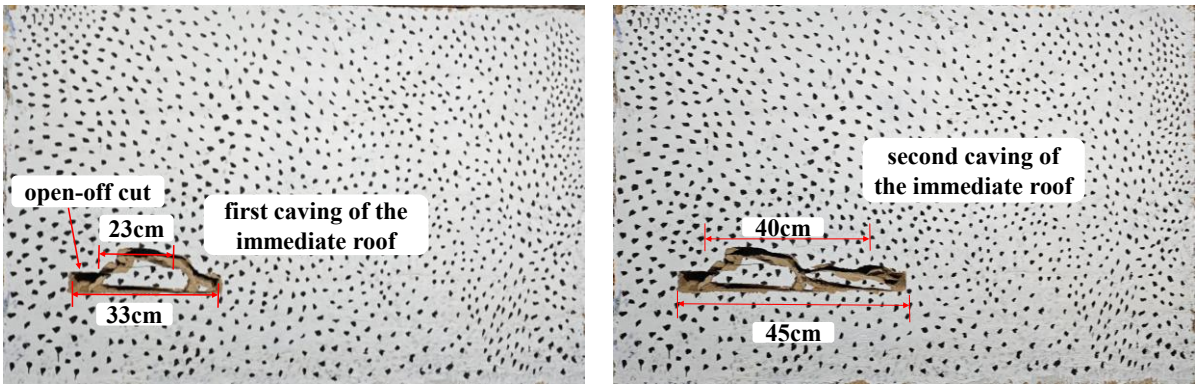
4.1. Fracture and crack evolution characteristics of overlying strata during extraction under an unweakened roof

A 15-cm-wide entry protection coal pillar was reserved on each side of the model, the open-off cut was arranged 15 cm from the left boundary of the model, and the working face advanced segment by segment from left to right with a single excavation step of 10 cm. As the exposed span of the goaf roof increased, the overlying loads were continuously transferred downward; when the accumulated stress exceeded the strength threshold of the strata, cracks developed gradually and the main roof fractured and subsided.

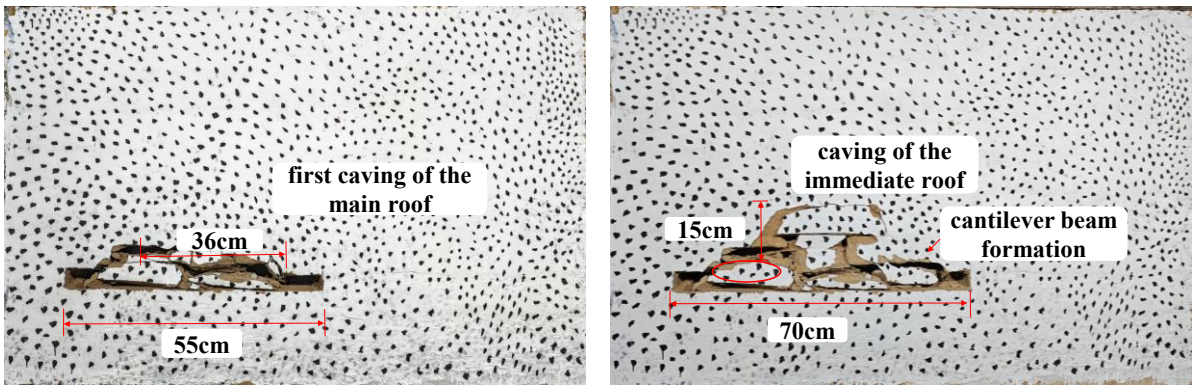
When the face advanced to 33 cm, the immediate roof fractured and caved for the first time, with a caved segment about 20 cm long and 3 cm high; afterwards, the immediate roof entered the periodic caving stage. When the face advanced to 45 cm, the second fracture occurred with a caved segment about 16 cm long, as shown in Fig. 6(a). When the face advanced to 55 cm, the overlying strata fractured as a whole and subsided in a layered manner, and the main roof caved for the first time (caved segment about 36 cm long and 7 cm high), with accompanied cracks developing above the goaf. When the face advanced to 70 cm, the third fracture of the immediate roof occurred (segment about 17 cm long), and fracture and bed separation appeared in Key Stratum 1 at about 15 cm above the goaf, with a separation zone about 25 cm long, as shown in Fig. 6(b). After its initial fracture, the main roof existed in the form of a cantilever beam. When the face advanced to 80 cm, the fourth fracture of the immediate roof occurred, and the main roof fractured periodically at the same time (segment about 26 cm long and 6 cm high); the broken rock blocks piled up in the goaf in layers in the form of a 'voussoir beam'. When the face advanced to 100 cm, the zone 30–90 cm from the rear of the goaf was compacted and filled by broken rock mass and the interlayer cracks tended to close, while the layered cracks within 5–30 cm behind the working face were still well developed, as shown in Fig. 6(c). When the extraction was completed at 110 cm, the cantilever beam and articulated beam structures over the goaf fractured and subsided successively, and the cumulative fracture lengths of the immediate roof, the main roof, and Key Stratum 1 were about 104 cm, 87 cm, and 60 cm, respectively. Significant interlayer cracks developed between Key Stratum 1 and the simulated basalt (Key Stratum 2) about 40 cm thick above it. After extraction, an additional load was applied to simulate the post-mining stress redistribution

equilibrium state. Before loading, there was an obvious gap between the caved roof and Key Stratum 2; after the load was applied, stress relief induced overall displacement and deformation of the roof, the caving profile of the overlying strata expanded symmetrically, and a load-transferring rock beam structure gradually formed above the face end. Local fracture occurred in Key Stratum 2, the cracks between Key Strata 1 and 2 tended to be compacted and closed, and the coal pillars on both sides were crushed under pressure. Key Stratum 2 exhibited bending subsidence and exerted a compaction effect on the gangue beneath it, and the goaf tended to become stable, as shown in Fig. 6(d).

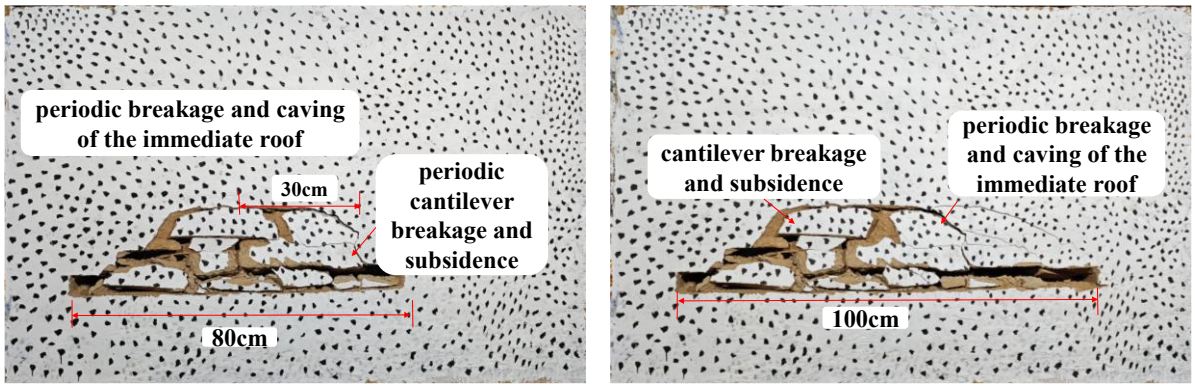
In summary, the physical simulation test of mining under a thick hard roof shows that bed separation of the immediate roof occurred at a face advance of 28 cm, and its first caving occurred at 33 cm (span about 20 cm, height about 3 cm); afterwards, periodic caving occurred at 45 cm, 70 cm, and 80 cm, with caving spans of about 16 cm, 17 cm, and 18 cm, respectively. The main roof first caved at 55 cm (span about 36 cm, height about 7 cm), and its periodic caving occurred at 80 cm (span about 26 cm, height about 6 cm). The first weighting interval of the immediate roof was about 33 cm and its average periodic weighting interval was about 17 cm; the first weighting interval of the main roof was nearly 55 cm and its periodic weighting interval was about 25 cm.



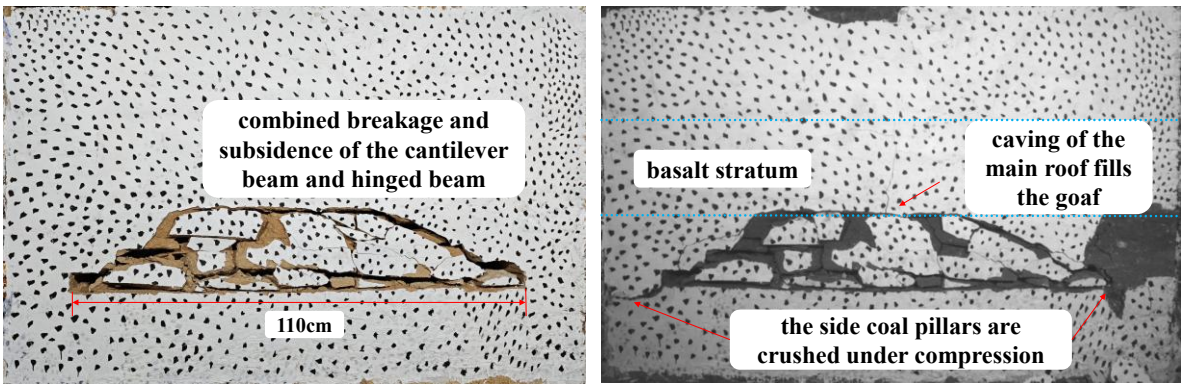
(a) face advance of 33 cm (33 m) and 45 cm (45 m)



(b) face advance of 55 cm (55 m) and 70 cm (70 m)



(c) face advance of 80 cm (80 m) and 100 cm (100 m)



(d) face advance of 110 cm (110 m) and the stress equilibrium state (110 m)

Fig. 6 Fracture, movement, and deformation characteristics of the overlying strata of the stope during conventional working face advance

4.2. Vertical stress variation characteristics of the overlying strata of the stope under an unweakened roof

Pressure cells were installed in the key strata and the coal seam of the similar simulation model to collect vertical stress data of the coal-rock strata. The vertical stress monitoring results are shown in Fig. 8, based on which the stress variation trends and distribution patterns of the surrounding rock of the stope during working face advance were analyzed.

Figure 7(a) shows that the stresses at monitoring points #1–#3 in the key strata all first increased and then decreased. The initial stress at basalt point #1 was about 0.17 MPa; after the coal seam was extracted starting from 15 cm on the left side, the stress increased slowly, and when the working face was about 10 cm from the point it rose sharply to a peak of 0.38 MPa, then decreased to 0.12 MPa and stabilized after the face had passed about 20 cm beyond

193 the point. The initial stresses at siltstone points #2 and #3 were 0.24 MPa and 0.25 MPa, respectively; their stresses
194 were stable at first and then increased sharply, reaching peaks of 0.54 MPa and 0.59 MPa, respectively, and both
195 decreased to about 0.15 MPa and stabilized after the face had passed about 20 cm beyond the points.
196 The records of sensors #4, #5, and #6 in the main roof (Fig. 7(b)) show that the stresses at points #4 and #5
197 remained generally stable until the working face was about 20 cm from the points, then rose rapidly to peaks of
198 about 0.68 MPa and 0.69 MPa, and dropped to 0.15 MPa and stabilized after the face had passed about 25 cm
199 beyond the points. Point #6 was arranged on the right side of the model; affected by the early roof caving, its stress
200 responded in advance: after about 20 cm of coal excavation, the stress accumulated and rose gradually, reached a
201 peak of 0.65 MPa at a face advance of 45 cm, then declined gradually with the continuing advance, and decreased
202 to 0.15 MPa and stabilized at 85 cm.
203 The monitoring results of points #7–#10 in the immediate roof and the coal seam are shown in Fig. 7(c). The initial
204 stresses at all points were about 0.26 MPa. At point #7 in the immediate roof, the stress surged to a peak of about
205 0.65 MPa when the working face was about 15 cm ahead of the point; afterwards, due to the caving of the weakened
206 roof, the stress decreased to 0.12 MPa and stabilized. The stresses at points #8 and #9 began to accumulate and
207 rise when the face was about 30 cm ahead, reaching peaks of 0.75 MPa and 0.71 MPa, respectively, and after the
208 face passed about 25 cm beyond the points, they dropped to about 0.15 MPa and stabilized. The data of point #10
209 in the coal seam show that when the working face was far away, the stress was not noticeably disturbed; the stress
210 began to accumulate when the face was about 35 cm ahead of the point, reached a peak of about 0.78 MPa at about
211 10 cm ahead of the point, and then dropped to zero because the coal seam was extracted and the sensor was
212 removed.
213 Overall, the monitoring scheme with pressure cells pre-embedded in the similar simulation test frame can finely
214 capture the stress distribution and evolution patterns of the surrounding rock of the stope throughout the whole
215 extraction process of the working face. The stress responses at all monitoring points share common characteristics:
216 the stress remained stable in the initial period; as extraction proceeded and the distance between the point and the
217 working face decreased, the stress gradually accumulated and rose; when the working face was within 10–20 cm
218 of the point, the stress jumped to its peak; and after further extraction made the face pass 20–30 cm beyond the
219 point, the stress unloaded rapidly and tended to stabilize. As for the vertical stress of the coal seam, the stress

started to rise when the working face was about 30 cm ahead of the point, reached a peak of about 0.78 MPa at 10 cm ahead of the working face, and then unloaded rapidly and gradually stabilized.

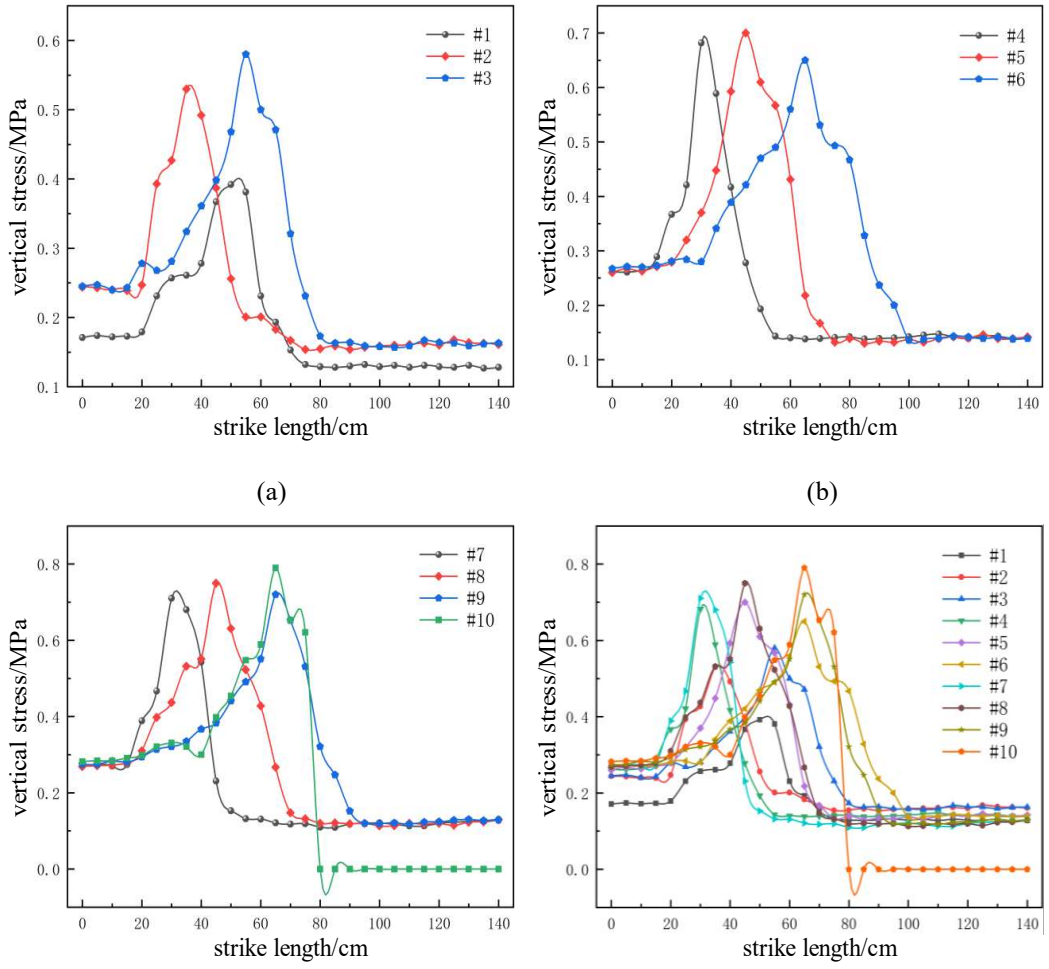


Fig. 7 Variation of the vertical stress distribution in the coal seam and its roof under normal working face excavation. (a) vertical stress variation curves of the basalt and siltstone, (b) vertical stress variation curve of the main roof, (c) vertical stress variation curves of the immediate roof and coal seam, (d) vertical stress variation curves of the coal-rock strata.

4.3. Fracture and crack evolution characteristics of overlying strata during extraction after roof weakening

The test scheme was to excavate the coal seam after pre-weakening of the roof. The roof was weakened by borehole pre-splitting, with a borehole spacing of 10 cm and a weakened layer thickness of 11 cm, as shown in Fig. 8. A 15-cm-wide coal pillar was reserved on each side of the model, the open-off cut was located on the left side 15 cm

from the boundary, and the face advanced gradually from left to right with an excavation length of 10 cm each time.

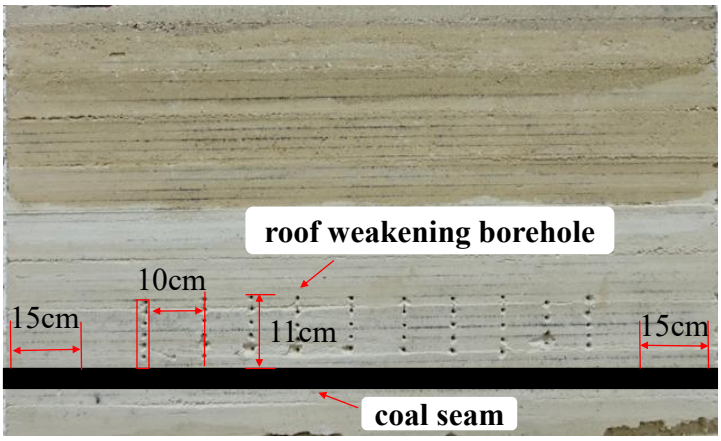
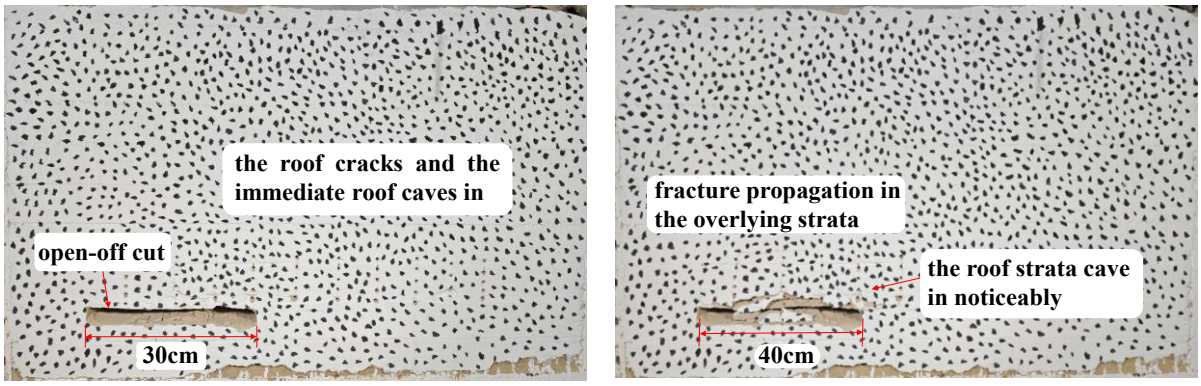


Fig. 8 Schematic diagram of borehole weakening of the model

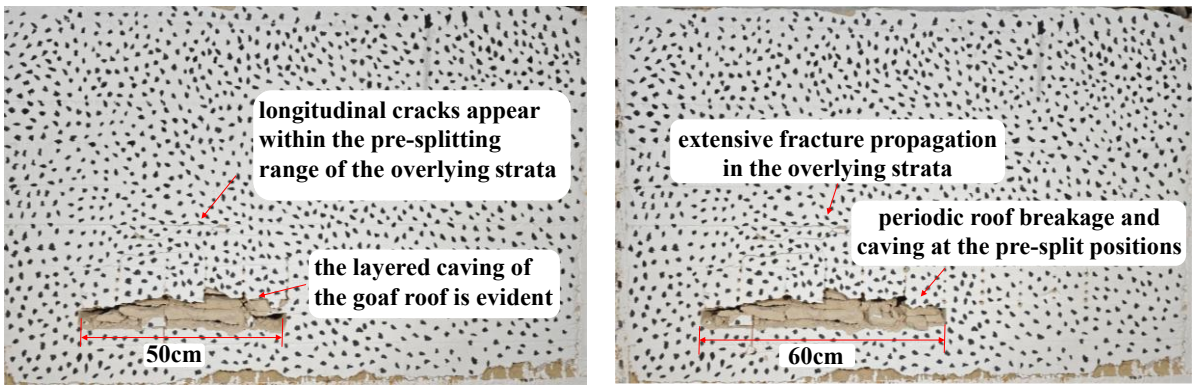
During the advance of the working face, the roof above the goaf gradually experienced crack propagation, interlayer detachment, and fracture and subsidence. When the excavation reached 30 cm, cracks appeared in the roof, and the immediate roof fractured and accumulated in the goaf. At 40 cm, the immediate roof continued to fracture and filled the goaf, with a fracture interval of 10 cm (consistent with the weakening spacing), and obvious horizontal cracks occurred in the stratum 11 cm above the coal seam, as shown in Fig. 9(a). At 50 cm, the roof caved in a layered manner with a span of about 35 cm, the horizontal cracks in the range of 11–20 cm continued to expand, and vertical cracks appeared at the pre-split borehole positions. At 60 cm, the roof in the pre-split zone responded with periodic fracture and caving, and the horizontal cracks in the overlying strata and the vertical cracks in the pre-split zone extended further, as shown in Fig. 9(b). When the face advanced to 70 cm, the goaf span continued to increase, the main roof fractured and caved to fill the goaf, and the caved rock mass existed in a layered form. The rock blocks near the working face hinged into articulated beams and cantilever beams, the bed separation of the basalt was significant, and the horizontal cracks in the overlying strata developed more intensively. When the simulated extraction advanced to 110 cm at the end stage, the main roof and the key strata fractured and caved in succession and accumulated in the goaf, and the caving characteristics showed that the fracturing of the roof along the pre-split positions was particularly prominent, as shown in Fig. 9(c). As shown in Fig. 9(d), an additional load was applied to the model to simulate the post-mining stress equilibrium state. It can be observed that after the goaf roof caved and was compacted, the cantilever beam structure on the working face side also failed, thereby reducing the load on the entry protection coal pillars. Clear transverse tensile cracks developed

above the basalt, indicating that as the goaf span increased, the hard thick stratum could undergo flexural subsidence and even fracture and caving.

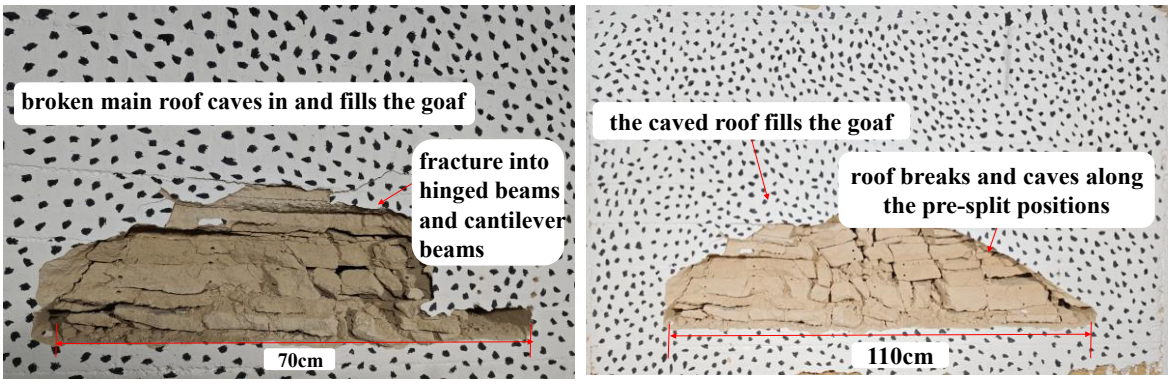
In summary, the excavation test with the pre-weakened roof shows that the roof did not cave immediately at the initial stage of extraction, but began its first fracture after the face advanced to 30 cm. Afterwards, for every 10 cm of advance, the roof fractured and caved periodically along the pre-split positions, indicating that although roof pre-weakening cannot make the roof cave immediately after extraction, it can effectively regulate the periodic fracturing behavior after the first caving occurs at the limit span, and the ultimate caving interval is significantly reduced. These results lay a foundation for the field application of the hydraulic fracturing roof weakening technology.



(a) face advance of 30 cm (30 m) and 40 cm (40 m)



(b) face advance of 50 cm (50 m) and 60 cm (60 m)



(c) face advance of 70 cm (70 m) and 110 cm (stress equilibrium state)

Fig. 9 Fracture, movement, and deformation characteristics of the overlying strata of the stope after roof weakening

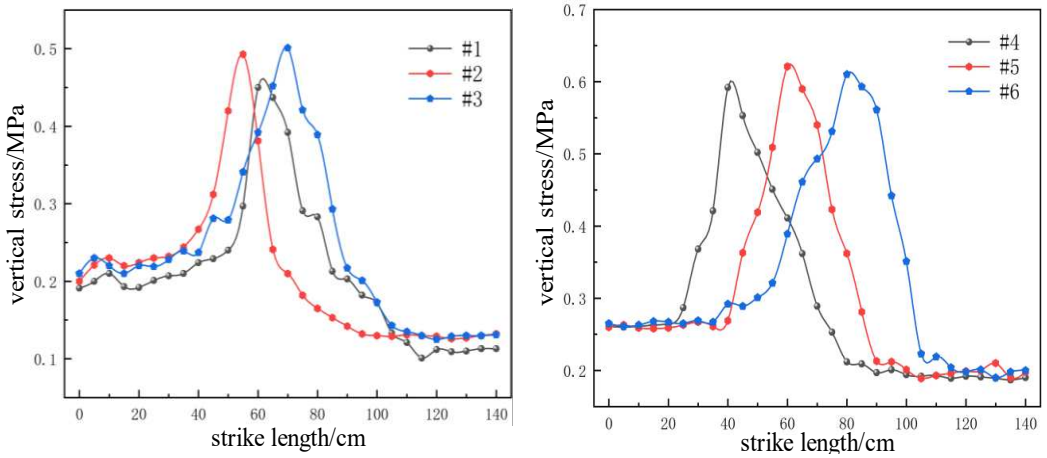
4.4. Vertical stress variation characteristics of the overlying strata of the stope after roof weakening

To clarify the distribution and evolution of the surrounding rock stress field of the stope under roof pre-weakening, pressure cells were pre-embedded in the key strata and the coal seam of the similar model; the roof was weakened first and then excavated, and the vertical stress variation curves of the coal-rock strata were obtained, as shown in Fig. 10.

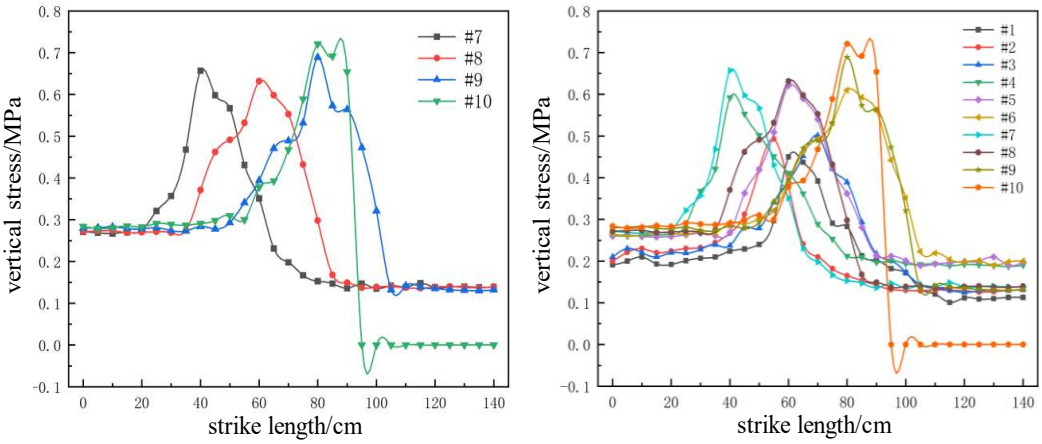
Figure 10(a) depicts the stress response trajectories of the monitoring points in the key strata (basalt and siltstone). The stresses at all points followed the basic pattern of 'rise → peak → decline'. Specifically, the initial stress at basalt point #1 was about 0.19 MPa; after the coal seam began to be extracted from 15 cm on the left side, the stress rose slowly at first, and when the working face was about 10 cm ahead of the point, it jumped sharply to a peak of about 0.45 MPa. After the face passed about 20 cm beyond the point, the stress recovered to near its initial value, then continued to decay slowly and remained stable after dropping to 0.11 MPa. The initial stresses at the two siltstone points #2 and #3 were 0.20 MPa and 0.21 MPa, respectively. As extraction advanced, their stresses first fluctuated slightly and then rushed to peaks of 0.49 MPa and 0.51 MPa; when the working face advanced to about 20 cm behind the points, the stresses returned to their initial values and then decreased to about 0.13 MPa and tended to stabilize.

As shown in Fig. 10(b), the stress curves of points #4, #5, and #6 in the main roof showed similar trends, differing only in the strike positions corresponding to their peaks. The stress evolution can be described in stages as follows: the stress remained generally stable in the initial stage; when the working face advanced to about 20 cm ahead of

292 the points, the stress rose rapidly to peaks of 0.59 MPa, 0.62 MPa, and 0.60 MPa, respectively; afterwards, as
293 extraction continued to about 30 cm behind the points, the stress dropped to about 0.2 MPa and remained stable.
294 The records of points #7–#10 in the immediate roof and the coal seam (Fig. 10(c)) show that the initial stresses at
295 the three points in the immediate roof were all close to 0.27 MPa. The stresses adjusted slowly in the initial stage;
296 when the working face advanced to 15 cm ahead of the points, they rose rapidly to their respective peaks, which
297 were 0.66 MPa, 0.62 MPa, and 0.68 MPa at the three points. As the immediate roof gradually caved into the goaf
298 under the influence of mining, the stresses unloaded abruptly and tended to level off. For the point located in the
299 coal seam, the initial stress was 0.28 MPa. When the working face was far from the point, the stress response was
300 not obvious; when the face was about 30 cm ahead of the point, the stress began to climb, reached a peak of about
301 0.72 MPa at 10 cm ahead, and then suddenly dropped to zero as the face continued to advance and exposed the
302 point.
303 Overall, after the pre-weakening treatment, the immediate roof and the main roof could fracture rapidly and fill
304 the goaf soon after excavation, and the vertical stresses decayed rapidly and returned to a stable state after peaking.
305 The weakened roof caved rapidly and compactly filled the goaf, providing a load-bearing and supporting effect on
306 the key strata (basalt and siltstone), and the compacted body effectively suppressed the stress concentration in the
307 coal seam caused by the large-area suspension of the roof. Combined with Fig. 10(d), it can be intuitively seen
308 that the stress of the surrounding rock of the stope generally exhibited a dynamic evolution pattern of 'slow rise –
309 rapid increase – peak – rapid decline – stabilization'. Among them, the vertical stress of the coal seam began to
310 rise when the working face was about 35 cm ahead of the point, reached a peak of about 0.72 MPa at 10 cm ahead,
311 and then declined sharply and gradually tended to a stable state.



312 (a) (b)
313



(c) (d)

Fig. 10 Variation of the stress distribution in the coal seam and its roof during working face excavation. (a) stress variation curves of the siltstone and basalt, (b) stress variation curve of the main roof, (c) stress variation curves of the immediate roof and coal seam, (d) stress variation curves of the coal-rock strata.

5. Conclusion

Based on similar material simulation tests, this study simulated the segment-by-segment extraction of the coal seam, systematically analyzed the movement and fracture characteristics of the overlying strata and the dynamic stress evolution of the surrounding rock of the stope, and compared the caving behavior of the overlying strata and the stress distribution differences before and after roof pressure relief. The following conclusions are drawn:

(1) In terms of caving control of the overlying strata, for the unweakened thick hard roof, the initial caving intervals of the immediate roof and the main roof are 33 m and 55 m, respectively, and the periodic caving intervals are 17 m and 30 m, respectively, which can easily lead to a large-area suspended roof. After borehole pre-splitting weakening, the initial caving interval is slightly shortened, and the roof fractures periodically along the pre-split weak planes for every 10 m of working face advance, which can completely avoid the dynamic disaster risks caused by long-distance roof suspension.

(2) In terms of mining-induced stress response, under the unweakened roof condition, the peak vertical stress in the coal seam is 0.78 MPa, with stress concentration occurring 30 m ahead of the working face; after pre-splitting weakening, the peak stress decreases to 0.72 MPa and the advance influence range is 35 m. The caved gangue fills the goaf and changes the load transfer path, transforming the 'concentrated pressure bearing of the suspended roof' into 'diffused pressure bearing of the filling body', so that the stress gradient becomes gentle and the strong ground pressure manifestation is effectively alleviated.

(3) Pre-splitting weakening improves the stress state of the key strata. The artificial pre-split cracks guide the orderly layered caving of the roof, and the gangue cushion provides continuous support to the basalt key stratum and inhibits the overall fracture of the hard strata. In the post-mining stress redistribution stage, the load on the coal pillars at both sides decreases, and the overall stability of the surrounding rock of the working face is improved. The conclusions can directly guide the field application of hydraulic pre-splitting and hydraulic fracturing for basalt-type thick hard roofs in southwestern China.

CRediT authorship contribution statement

Chun Zhao: Methodology, Writing – original draft. **Zhenqian Ma**: Conceptualization, Supervision, Writing – review & editing, Project administration, Funding.

Acknowledgements

The work presented in this paper was supported by the projects of the "National Natural Science Foundation of China (52274116)", "Guizhou Provincial Program on Commercialization of Scientific and Technological Achievements (LH[2024]ZHONGDA024)" and "Guizhou Provincial Key Technology R&D Program (KJFZ[2025]009)".

Data availability

Data will be made available on request.

Conflicts of Interest:

The authors declare no conflict of interest.

References

[1] XIE Heping, WU Lixin, ZHENG Dezhi. Prediction on the energy consumption and coal demand of China in 2025[J]. *Journal of China Coal Society*, 2019, 44(7): 1949-1960.

[2] XIE Heping, WANG Jinhua, WANG Guofa, et al. New ideas of coal revolution and layout of coal science and technology development[J]. *Journal of China Coal Society*, 2018, 43(5): 1187-1197.

[3] YUAN Liang. Strategic thinking of simultaneous exploitation of coal and gas in deep mining [J]. *Journal of China Coal Society*, 2016, 41(1): 1-6.

[4] JixiongZhang, BaiyiLi, NanZhou, Qiang Zhang. Application of solid back filling to reduce hard-roof caving and long wall coal face burst potential [J]. International Journal of Rock Mechanics & Mining Sciences, 2024, 88 : 197-205.

[5] XIE Heping, GAO Feng, JU Yang. Research and development of rock mechanics in deep ground engineering [J]. *Chinese Journal of Rock Mechanics and Engineering*, 2015, 34(11): 2161-2178.

[6] LIN H F, LIU S B, SHUANG H Q, et al. Overburden rock fracture evolution law and pressure relief gas extraction technology of gob-side entry retaining mining [J]. *Journal of Mining and Strata Control Engineering*, 2024, 6(1): 013537.

[7] HAN C L, ZHANG N, RAN Z, et al. Superposed disturbance mechanism of sequential overlying strata collapse for gob-side entry retaining and corresponding control strategies [J]. *Journal of Central South University*, 2018, 25(9): 2258-2271.

[8] DONG H J, LIU Y L, WU Z K, et al. Determination and application of filling body parameters of flexible moulded pier columns for gob-side entry retaining in fully mechanized caving ace with large mining height[J]. *Metal Mine*, 2024(12): 52-59.

[9] KANG X T, GAO L, LUO F, et al. Application of digital speckle technology in similar simulation test of coal mine[J]. *Journal of Safety Science and Technology*, 2020, 16(11): 140-146.

[10] LIANG D, LI D, XUE F, et al. Innovative project based on digital image correlation technology and infrared thermal imaging technology[J]. *Experimental Technology and Management*, 2019, 36(12): 232-235.

[11] YAO Hai, WANG Ning. Similar simulation on fully mechanized top-coal caving mining in lower slicing of compound coal seam[J]. *Coal Engineering*, 2021 ,53(3): 11-15.

[12] SUN Xueyang, LIU Liangdong, LI Cheng, et al. Studyon influence of layered mining of extra thick coal seamon faults based on similar materials test[J]. *Coal Science and Technology*, 2019, 47(2): 35-40.

[13] ZHAI Xinxian, ZHAO Xiaofan, ZHAI Yanwei, et al. Separation and fracturing mechanical models of overlying hugely-thick conglomerate stratum in fully mechanized caving mining and their application [J].*Journal of China University of Mining & Technology*, 2023, 52(2): 241-254.

[14] ZHAI Xinxian, ZHAO Xiaofan, TU Xingzi, et al. Study on the deformation movement law of hugely-thick conglomerate stratu mover longwall top coal caving[J]. *Journal of Henan Polytechnic University* (Natural Science), 2019, 38(3): 16-23.

[15] CHAI J, YANG Y Y, OUYANG Y B, et al. Comparison of optical measurement methods for deformation and failure simulation test of overburden in working face[J]. *Journal of China Coal Society*, 2021, 46(1): 154-163.

[16] Zhang Hanrui, Liu Changyou, Liu Huaidong, et al. Study on asymmetric floor heave mechanism and hydraulic fracturing control in roadways under mining disturbance[J]. *Journal of Mining & Safety Engineering*, 2026, 43(02): 307-317.

[17] Shi Zhihan, Liu Xuesheng, Gao Yudong, et al. Protection technology of soft rock main roadway with advanced roof cutting and pressure relief in large mining height face of kilometer deep mine[J]. *China Mining Magazine*, 2025, 34(05): 163-175.

[18] Wang Junyao, Shen Jianjun, Zeng Yifan, et al. Study on multi-factor coupling effect of similar simulation material based on RSM[J/OL]. *Coal Science and Technology*, 1-12[2026-04-08].

[19] Dou Linming, Kan Zihao, Cao Anye, et al. Dynamic physical simulation similarity principle of coal/rock for coal burst[J]. *Journal of China Coal Society*, 2026, 51(01): 274-292

[20] Ning Shan, Zhu Weibing, Xu Jialin, et al. Simulation study on damage and fracture evolution of extra-thick key stratum based on carbon fiber composite material[J/OL]. Coal Science and Technology, 1-17[2026-04-08].

[21] Li Zhihua, Yang Ke, Chen Denghong. Development of a simulation device for unconsolidated confined aquifers and experimental teaching[J]. Experimental Technology and Management, 2025, 42(11): 179-186.